Journal of Alloys and Compounds 527 (2012) 219–225

Contents lists available at SciVerse ScienceDirect

Journal of Alloys and Compounds

journal homepage: www.elsevier.com/locate/jallcom

Bulk modulus and thermal properties of RVO_3 (R = La, Ce, Pr, Nd)

N.K. Gaur, Atahar Parveen*

Department of Physics, Barkatullah University, Bhopal 462026, India

ARTICLE INFO

Article history:
Received 6 February 2012
Received in revised form 24 February 2012
Accepted 25 February 2012
Available online xxx

Keywords:
Perovskites
Cohesive energy
Bulk modulus
Specific heat

ABSTRACT

We have investigated the bulk modulus and thermal properties of orthovanadates RVO_3 (R = La, Ce, Pr, Nd) probably for the first time in both monoclinic and orthorhombic phase by incorporating the effect of lattice distortions using the Modified Rigid ion model (MRIM). The calculated bulk modulus, specific heat and other thermal properties reproduce well with the available experimental data, implying that MRIM represents properly the nature of the perovskite type vanadates. The specific heat results can further be improved by including the spin and orbital ordering contributions to the specific heat.

Published by Elsevier B.V.

1. Introduction

The RVO_3 compounds (R = La, Ce, Pr, Nd) often referred to as orthovanadates are typical t_{2g} electron systems which form a very interesting system that exhibits outstanding physical properties, as anomalous diamagnetism and an almost simultaneous crystallographic-antiferromagnetic transition, as a consequence of the comparable spin–spin and orbital–lattice interactions [1]. These compounds exhibit unusual magnetic properties such as a temperature induced magnetization reversal [2], staircase like and glassy like behavior in the magnetization [3] and magnetic memory effects [4,5]. The magnetic properties of the orthovanadates have been well studied; but a systematic study on the physical, thermodynamic and elastic properties on all the compounds of the series is lacking [1]. The purpose of this paper is to provide a complete basis for the theoretical description of the elastic and thermal properties of the vanadates. At room temperature these materials exhibit the orthorhombic $GdFeO_3$-type structure with space group *Pbnm* [6–15] resulting from a cooperative distortion of the VO_6 octahedra. The temperature driven structural phase transition from an orthorhombic to a monoclinic structure, with space groups *Pbnm* and $P2_1/b11$, respectively [7–9], motivates to probe the lattice dynamics associated with these structural changes. In this paper we report a detailed study of elastic, cohesive and thermal properties in perovskite type vanadium oxides, RVO_3 (R = La, Ce, Pr, Nd).

$LaVO_3$ the first compound of the series exhibits many exciting properties which can be related to orbital and spin rearrangements [15]. It has been studied extensively in terms of its structural changes but there still exist a number of issues which have yet to be resolved [3]. Most outstanding points of dispute concern its structures above and below the transition temperature and nature of two phase transitions. Structural studies by means of synchrotron X-ray measurements have confirmed that at T_2 there is an abrupt change in the lattice parameters associated with the first order crystallographic phase transition from orthorhombic *Pbnm* to monoclinic $P2_1/b11$ symmetry with decreasing temperature [7]. Since the structural change from orthorhombic to monoclinic symmetry is usually accompanied by orbital ordering (OO), T_2 is identified as the OO temperature [14]. On the other hand, at T_1, there is only a slight variation reported for the lattice parameters which does not result in any change in the crystallographic symmetry [3]. $CeVO_3$ plays a special role in the family RVO_3. In line with other members of the series, this compound also exhibits two structural phase transitions, with decreasing temperature it undergoes a second order phase transition at $T_o = 154$ K with crystal symmetry lowered to monoclinic $P2_1/b11$, induced by *G*-type orbital ordering, and a first order phase transition at the Neel temperature T_N, accompanied by a sudden lattice change. The *C*-type antiferromagnetic ordering enhances the cooperative JT distortion, resulting in a spontaneous change in the crystal structure [3,8]. It is thus interesting to explore the elastic and thermal properties of $CeVO_3$.

$PrVO_3$ and $NdVO_3$ retain their orthorhombic structure down to $T_{OO} = 185$ K. Here, the symmetry changes to monoclinic $P2_1/b11$, identified with the onset of OO. Below the transition temperature, T_N for $PrVO_3$ and $NdVO_3$ the canting of spins gives rise to a ferromagnetic component. The value of the monoclinic angle increases with decreasing temperature, before stabilizing shortly below T_N in $PrVO_3$ and $NdVO_3$. For both compounds, the onset of the OO is not really accompanied by a change in the unit cell volume. The V–O distances provide evidence that the room temperature

* Corresponding author. Tel.: +91 755 2491821; fax: +91 755 2491823.
E-mail address: ataharparveen@gmail.com (A. Parveen).

0925-8388/$ – see front matter. Published by Elsevier B.V.
doi:10.1016/j.jallcom.2012.02.173

phase is orbitally disordered and the low-temperature phase is orbitally ordered [6]. At room temperature the RVO_3 (R = La, Ce, Pr, Nd) compounds possess orthorhombic structure where all V sites are equivalent, while two independent V sites exist in the monoclinic structure. These two V sites form alternate layers along the *c* axis. Above the transition all the VO_6 octahedra are tilted around the three crystallographic axes and are elongated along the [1 1 0] direction. The elongation increases below the transition and occurs in different directions, 90° apart, in the two V sites in the monoclinic structure. This observed arrangement of the elongated VO_6 octahedra at low temperature strongly supports the existence of the *G*-type orbital ordering below the transition [3]. It is well established that lattice effect play an important role in determining the spin and charge order properties in vanadates and they are generally described by the strain related to Jahn–Teller (JT) type distortions [10] of the VO_6 octahedra and their tilts. The relation of this dynamic JT distortion with the bulk modulus and thermal properties is also considered in the present work. The effect of lattice distortions on the elastic and thermal properties of these Vanadates has been investigated by an atomistic approach.

Earlier, we have used the MRIM successfully to study the thermal properties of some perovskite manganites and other inorganic compounds over a fairly wide range of temperatures [16–18] which motivated us to describe the bulk modulus, cohesive and thermal properties of the RVO_3 (R = La, Ce, Pr, Nd) compounds. The study of the lattice thermal properties of these compounds may be taken as starting point for the consistent understanding of the more complex physical properties of the perovskite type rare earth orthovanadates. The essentials of the MRIM formalism and the results obtained from its application are presented in subsequent sections.

2. Formalism of MRIM

The major contribution to pair potential of modified rigid ion model (MRIM) is long-range (LR) Coulomb attractions which are counter balanced by the short-range (SR) Hafemeister–Flygare-type (HF) [19] overlap repulsion operative up to the second nearest neighbor atoms and the van der Waals attraction due to dipole–dipole (d–d) interactions, whose coefficients are estimated from Slater–Kirkwood Variational (SKV) [20] approach. The formalism of MRIM has been derived for the following effective interatomic potential.

$$\phi = \frac{-e^2}{2}\sum_{kk'} Z_k Z_{k'} r_{kk'}^{-1} - \sum_{kk'} C_{kk'} r_{kk'}^{-6} + \sum_i \left[n_i b_i \beta_i^{kk'} \exp\left\{ \left(\frac{r_k + r_{k'} - r_{kk'}}{\rho_i} \right) \right\} + b_i n' \beta_i^{kk} \exp\left\{ \left(\frac{2r_k - r_{kk}}{\rho_i} \right) \right\} + b_i \frac{n_i'}{2} \beta_i^{k'k''} \exp\left\{ \left(\frac{2r_{k'} - r_{k'k'}}{\rho_i} \right) \right\} \right] \quad (1)$$

The symbols involved are the same as those defined in our earlier papers [16–18]. Here $r_{kk'}$ appearing in the first term on the right represents the separation between the nearest neighbors while r_{kk} and $r_{k'k'}$ appearing in the next two terms are the second neighbor separations. r_k ($r_{k'}$) is the ionic radius of the k (k') ion. n (n' and n'') are the number of nearest (next nearest) neighbor ions. In ABO_3 (like $LaVO_3$) perovskite structure, k represents the cation (A, B) and k' denotes the type (O_1, O_2) of the ion. The summation is performed over the ion pair (A–O) and (B–O). b_i and ρ_i are the hardness and range parameters for the ith cation–anion pair ($i = 1, 2$) respectively and $\beta_i^{kk'}$ is the Pauling coefficient [21] given by

$$\beta_i^{kk'} = 1 + \left(\frac{Z_k}{N_k}\right) + \left(\frac{Z_{k'}}{N_{k'}}\right) \quad (2)$$

Z_k ($Z_{k'}$) and N_k ($N_{k'}$) are the valence and the number of electrons in the outermost orbit of the k (k') ion respectively. The contributions of van der Waal's (vdW) attraction for the dipole–dipole interaction is determined by using Slater–Kirkwood Variational (SKV) method [20]

$$\phi_{kk'}^{VdW} = C_{kk'} r_{kk'}^{-6}$$

and

$$C_{kk'} = \frac{3eh}{4\pi m}\alpha_k \alpha_{k'} \left[\left(\frac{\alpha_k}{N_k}\right)^{1/2} + \left(\frac{\alpha_{k'}}{N_{k'}}\right)^{1/2} \right]^{-1} \quad (3)$$

Here e and m are the charge and mass of the electron respectively. α_k ($\alpha_{k'}$) is the polarizability of k (k') ion. N_k ($N_{k'}$) are the effective number of electrons responsible for the polarization of k (k') ion.

The model parameters, hardness (b) and range (ρ) are determined from the equilibrium condition.

$$\left[\frac{d\phi}{dr}\right]_{r=r_0} = 0 \quad (4)$$

and the bulk modulus

$$B = \frac{1}{9Kr_0}\left[\frac{d^2\phi}{dr^2}\right]_{r=r_0} \quad (5)$$

where K is the crystal structure-dependent constant and r_0 is the equilibrium nearest neighbor distance. The expressions for calculating the thermodynamic properties like Debye temperature and Gruneisen parameter are taken from our earlier papers [16–18].

Eqs. (4) and (5) have been used to compute the model parameters which are used to calculate the cohesive and thermal properties of these vanadates.

Table 1
The cation radius at A-site, tolerance factor, bulk modulus and lattice distortions of $LaVO_3$ and $CeVO_3$ at room temperature.

Compound	$LaVO_3$	$CeVO_3$	$PrVO_3$	$NdVO_3$
r_k (Å) (A-site)	1.16	1.143	1.13	1.11
Tolerance factor (t)	0.886	0.880	0.874	0.868
JT distortion (Δ_{JT})	0.0576	0.0571	0.0570	0.0563
Charge mismatch, σ_C	1.00	1.00	1.00	1.00
Size mismatch, σ_m	1.813	1.786	1.759	1.733
Octahedra rotation, φ_S	0.980	0.976	0.961	0.973

3. Results and discussions

3.1. Model parameters

The values of input data like unit cell parameters (a, b, c) and other interionic distances are taken from Refs. [1,5–8,15,22–24] for RVO_3 (R = La, Ce, Pr, Nd) and this data is used for the evaluation of model parameters (b_1, ρ_1) and (b_2, ρ_2) using Eqs. (4) and (5). The oxygen atoms are considered to be polarizable and vdW coefficients $C_{kk'}$ were calculated using SKV method [21]. The values of average cation radius at A-site are listed in Table 1. The values of model parameters (b_1, b_2, ρ_1 and ρ_2) at various temperatures calculated for two different phases (monoclinic and orthorhombic) for RVO_3 (R = La, Ce, Pr, Nd) compounds are listed in Tables 2 and 3. The values of model parameters b_1 and ρ_1 are for the ion pairs V^{3+}/V^{4+}–O^{2-} and those of b_2 and ρ_2 are for the ion pairs R^{3+}–O^{2-}.

Table 2
Model parameters and bulk modulus based on AIM theory for $LaVO_3$ and $CeVO_3$ as a function of temperature in monoclinic and orthorhombic phase.

Compound	T (K)	ρ_1 (Å) (V–O)	$b_1 \times 10^{-19}$ (J) (V–O)	ρ_2 (Å) (R–O)	$b_2 \times 10^{-19}$ (J) (R–O)	B_0 (Gpa) (AIM)
Monoclinic phase						
$LaVO_3$	5	0.281	1.501	0.438	0.193	96.01
	80	0.280	1.498	0.436	0.193	96.18
	140	0.278	1.487	0.433	0.191	96.46
$CeVO_3$	5	0.297	1.769	0.441	0.223	96.19
	80	0.283	1.688	0.422	0.214	97.97
	140	0.270	1.610	0.404	0.204	99.57
Orthorhombic phase						
$LaVO_3$	180	0.264	1.520	0.413	0.197	99.02
	260	0.258	1.553	0.406	0.202	100.02
	295	0.245	1.501	0.386	0.196	106.73
$CeVO_3$	180	0.270	1.620	0.404	0.206	99.71
	260	0.266	1.618	0.398	0.206	100.23
	295	0.254	1.557	0.382	0.199	106.33

3.2. Cohesive energy

We have calculated the cohesive energy of RVO_3 (R = La, Ce, Pr, Nd) compounds using Eq. (1) and then reported them in Tables 4 and 5. The calculated cohesive energy shows the magnitude of cohesion in these compounds and indicates a measure of strength of the forces binding atoms together in solids. The cohesive energy is therefore expected to change in the same trend as the bulk modulus, which represents the strength to the volume change and is related to the overall atomic binding properties of the materials. The negative values of cohesive energy show the stability of these compounds. The present cohesive energy for $LaVO_3$ is closer to the reported value of Khan and Akhtar [24]. Other cohesive energy values for $CeVO_3$, $PrVO_3$ and $NdVO_3$ could not be compared due to lack of experimental data but the magnitude are found to be in the range often found in perovskite structure materials. To test the validity of our model the lattice energies for these compounds were calculated using the generalized Kapustinskii equation [25] on the lines of our earlier papers [16–18].

3.3. Bulk modulus

We have determined the bulk modulus of RVO_3 (R = La, Ce, Pr, Nd), systematically on the basis of formulations of atoms in molecules (AIM) theory which emphasize the partitioning of static thermodynamic properties in condensed systems into atomic or group contributions. Since all AIM atomic properties are assumed to be additive and quantum atoms fill the space, bulk or thermodynamic properties may be partitioned into atomic or group contributions.

$$k = \sum_i f_i k_i \quad \text{and} \quad \frac{1}{B} = \sum_i f_i \frac{1}{B_i} \tag{6}$$

where $f_i = (V_i/V)$

We considered that the molar volume V can be written as the sum over atomic volumes (V_i), f_i is the fractional volume occupancy due to quantum subsystem i in a unit formula volume, B is bulk modulus of the compound and K is its compressibility. Here we have considered oxygen atoms as the bulkiest and most compressible and its local compressibility varies according to the varying cation volumes and their relative occupying factor f_i on the lines of Pendas et al. [26]. The oxide ions are treated as plastic constituents of these structures. The values of atomic radii are taken from Ref. [22] and the data on atomic compressibility was taken from Ref. [27]. The values obtained are represented as B_0 in Tables 2 and 3.

The versatility of the perovskite structure, with general formula ABO_3, is based on the ability of the AX_3 packing to accommodate a large variety of A and B cations with different A–O and B–O distances. For simple oxide perovskites ABO_3, the symmetry of the resultant compound can be anticipated through the geometrical relationship between both cation–anion distances [28]. As the cation radius decrease down the series, the Goldschmidt tolerance factor t ($t = (r_A + r_O)/2(r_B + r_O)$) whose value for cubic perovskite structure is around 1 [29,30], also reduces (Table 1) so the structure progressively deviates from the orthorhombic to highly distorted orthorhombic and a decrease in the unit cell volume can be observed. This decrease in cell volume corresponds to increase in bulk modulus of the compound.

Table 3
Model parameters and bulk modulus calculated using AIM theory for $PrVO_3$ and $NdVO_3$ in monoclinic and orthorhombic phase as a function of temperature.

Compound	T (K)	ρ_1 (Å) (V–O)	$b_1 \times 10^{-19}$ (J) (V–O)	ρ_2 (Å) (R–O)	$b_2 \times 10^{-19}$ (J) (R–O)	B_0 (Gpa) (AIM)
Monoclinic phase						
$PrVO_3$	5	0.275	1.562	0.417	0.197	108.5
	80	0.264	1.459	0.395	0.185	109.9
	140	0.247	1.338	0.370	0.171	112.3
$NdVO_3$	5	0.258	1.392	0.382	0.176	114.6
	80	0.248	1.323	0.367	0.168	116.0
	140	0.239	1.262	0.354	0.160	117.2
Orthorhombic phase						
$PrVO_3$	180	0.238	1.285	0.346	0.164	113.5
	260	0.235	1.274	0.354	0.163	113.8
	295	0.234	1.270	0.352	0.163	113.9
$NdVO_3$	180	0.233	1.228	0.346	0.156	117.8
	260	0.231	1.208	0.340	0.154	118.0
	295	0.225	1.188	0.335	0.151	118.1

Table 4
Cohesive and thermal properties of $LaVO_3$ and $CeVO_3$ in monoclinic and orthorhombic phase, as a function of temperature.

Compound	T (K)	B_T (GPa)	ϕ (eV)	ϕ (eV) (kapustinskii equation)	θ_D (K)	γ
Monoclinic phase						
$LaVO_3$	5	178.50	−143.83	−143.65	509.32	1.87
	80	178.88	−144.30	−143.95	510.24	1.88
	140	179.47	−144.63	−143.97	511.88	1.90
$CeVO_3$	5	176.71	−144.07	−143.86	502.51	1.79
	80	179.30	−144.56	−144.69	511.42	1.91
	140	182.66	−144.58	−145.41	521.06	2.04
Orthorhombic phase						
$LaVO_3$	180	183.38	−144.68	−145.16	522.47	2.06
	260	185.18	−144.71	−145.77	526.73	2.13
	295	197.48	−145.00	−146.09	544.76	2.28
Others	300	194[a]	−140.76[b]			
O_3	300				553[c]	
VO_3	180	182.48	−144.07	−145.61	520.97	2.04
	260	183.80	−144.58	−146.12	524.04	2.08
	295	194.60	−145.47	−146.67	539.54	2.20
Others	300	186[a]				(2–3)[d]

[a] Ref. [13].
[b] Ref. [24].
[c] Ref. [16].
[d] Ref. [32].

We considered the effect of charge and size mismatch along with the octahedral distortions due to Jahn–Teller effect on the bulk modulus of the compounds [16,17]. These factors will determine the change in the unit cell volume which in turn will change the global bulk modulus of the compound. In the high-temperature phase ($T > 200$ K) of RVO_3 the lattice distortions are away from the ideal cubic perovskite structure which are determined entirely by ionic-size effects, a strong cooperative Jahn–Teller effect is active in the low-temperature phase [31]. The formal expression for the JT distortion of VO_N ($N = 6$) octahedral is taken as

$$\Delta_{JT} = \sqrt{\left(\frac{1}{N}\right)\sum_{i}^{N}\left(\frac{d_i - \langle d\rangle}{\langle d\rangle}\right)^2} \tag{7}$$

where $\langle d\rangle$ is the average value of d_i bond distances in VO_6 octahedral. This distortion seems to be decreasing slightly down the series based on these four compounds and is reported in Table 1.

The expressions for the cation size and charge mismatch at the A-site and B-site is

$$\sigma_m = \left[\frac{(1 - x_A)r_A + x_A r_{A'}}{(1 - x_A)r_{V^{3+}} + x_A r_{V^{4+}}}\right] \tag{8}$$

where x_A is the concentration of the doped trivalent rare earth cation of radius $r_{A'}$ (CN = 8) at the A-site and $r_v{}^{3+}$ (CN = 6) is the radius of V^{3+} ion in valence state 3 and $r_v{}^{4+}$ (CN = 6) is the value in valence state 4. Similarly replacing the radius (r_A) with cation charge at A-site and B-site, the charge mismatch can also be calculated. The charge mismatch comes out to be unity for the pure compounds. The values are listed in Table 1.

The effect of buckling of angle V–O–V on distortions of the unit cell is calculated as

$$\phi_S = \cos\langle\omega\rangle = \cos\frac{\langle\pi\rangle - \theta}{2} \tag{9}$$

where average tilting of the VO_6 octahedral around pseudo-orthorhombic direction is $\langle\omega\rangle$ and $\langle\theta\rangle$ is the average tilting angle V–O–V.

Table 5
Cohesive and thermal properties of $PrVO_3$ and $NdVO_3$ in monoclinic and orthorhombic phase, as a function of temperature.

Compound	T (K)	B_T (GPa)	ϕ (eV)	ϕ (eV) (kapustinskii equation)	θ_D (K)	γ
Monoclinic phase						
$PrVO_3$	5	195.58	−146.05	−147.56	526.40	1.91
	80	199.25	−146.08	−148.29	537.68	2.05
	140	203.59	−146.12	−149.07	551.40	2.24
$NdVO_3$	5	205.19	−146.82	−147.82	545.50	2.12
	80	207.53	−146.91	−148.41	553.44	2.23
	140	209.60	−147.09	−149.04	560.63	2.33
Orthorhombic phase						
$PrVO_3$	180	205.15	−146.47	−149.47	557.56	2.33
	260	207.00	−147.06	−149.79	561.07	2.37
	295	208.45	−147.36	−149.94	563.17	2.39
Others	300	205[a]				
$PrMnO_3$	300				534.85[b]	
$NdVO_3$	180	212.07	−147.22	−147.41	566.06	2.40
	260	216.44	−147.50	−147.45	572.30	2.46
	295	220.67	−147.70	−147.53	578.05	2.50
Others	300					(2–3)[c]
$NdMnO_3$					545.34[b]	

[a] Ref. [13].
[b] Ref. [16].
[c] Ref. [32].

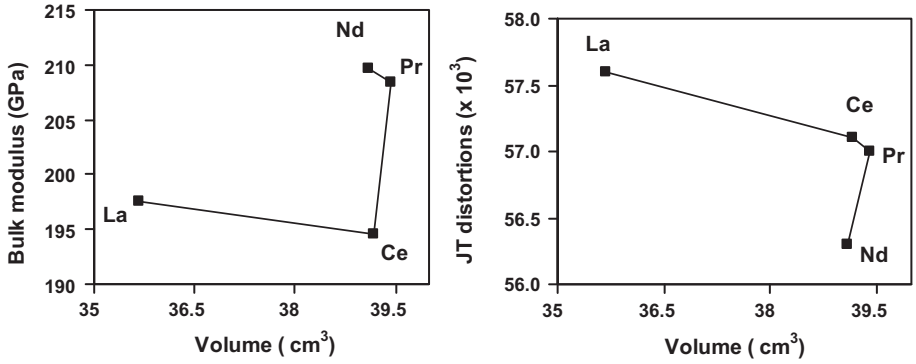

Fig. 1. Variation of (a) bulk modulus and (b) JT distortions of RVO_3 with molar volume (cm^3) of the basic perovskite cell.

It is now appropriate to propose the following relation for the bulk modulus of the distorted perovskite Vanadates

$$B_T = \frac{K_S B_0 \sigma_m \cos\omega}{\exp(\Delta_{JT})\sigma_C} \quad (10)$$

where K_S is the spin-order-dependent constant of proportionality and its value is less than one for ferromagnetic state, B_0 is the bulk modulus for undistorted structure calculated on the basis of AIM theory, σ_m is the size mismatch, σ_C is the charge mismatch, Δ_{JT} is JT distortion of VO_6 octahedral and cos (ω) is the effect of buckling of V–O–V angle. The values of various distortions are given in Table 1 and the value of bulk modulus of the distorted structure is also reported in Tables 4 and 5 as B_T which takes effect of all the distortions. The calculated values for B_T are in good agreement with the earlier reported experimental values [13] at room temperature for RVO_3 (R = La, Ce, Pr, Nd) compounds. We expect the bulk modulus to vary inversely with JT distortions; higher distortions of VO_6 octahedra will mean a lower value of the bulk modulus of the compound. As this distortion decreases down the series, the bulk modulus increases except for $CeVO_3$. Fig. 1 depicts the inverse relation of bulk modulus and JT distortions of RVO_3 (R = La, Ce, Pr, Nd) compounds.

3.4. Thermal properties

The concept of Debye temperature has played an important role in determining the thermophysical properties of materials. It is basically a measure of vibrational response of the material and is therefore intimately connected with properties like specific heat and thermal expansion. Our results on Debye temperature for RVO_3 (R = La, Ce, Pr, Nd), are probably the first reports on them hence could not be compared with others. The magnitude of calculated value of Debye temperature for RVO_3 (R = La, Pr, Nd) is in closer agreement with the perovskite structure manganites $RMnO_3$ (R = La, Pr, Nd) [16]. Here, it is to be noted that the higher value of Debye temperature indicate the higher phonon frequencies of these compounds. Fig. 2 shows the variation of Debye temperature for RVO_3 (R = La, Ce, Pr, Nd) with the calculated tolerance factor. It is clearly seen from Fig. 2 that the Debye temperature increases with change in R species down the series except for $CeVO_3$; which is less than that of $LaVO_3$. The Debye temperature estimated for the analysis of lattice specific heat is also reported in Tables 4 and 5.

The value of Gruneisen parameter (Table 2) seems to be reasonable since its value lies between 2 and 3 as reported earlier [32].

Very scant attention has been focussed on the specific heat study, while it is regarded as a useful technique for the study of thermo physical properties. The specific heat for RVO_3 (R = La, Ce, Pr, Nd) at temperature $1\,K \leq T \leq 300\,K$ are displayed in Figs. 3–6. It

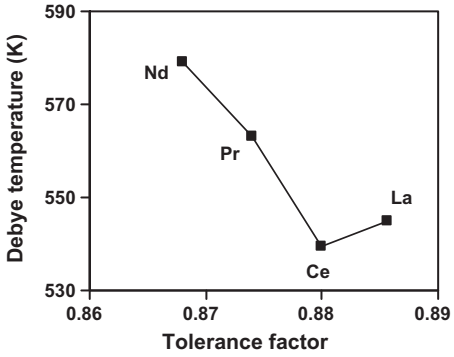

Fig. 2. Variation of Debye temperature with tolerance factor for RVO_3 compounds.

is seen from Fig. 3 that the calculated lattice specific heat of $LaVO_3$ is found to be in good agreement with the measured data of Tung et al. [2], except with the sharp peak. This peak gives the magnetic transition from paramagnetic (PM) to C type spin ordered state, where spins align ferromagnetically along the c axis and stagger in the ab plane, occurs at spin ordering temperature (T_{SO}). An inspection of Fig. 4 shows that the computed specific heat variation for $CeVO_3$ is closer to the experimental data [33]. Also, it is seen from this figure that the experimental results exhibits a sharp anomaly, which is formed by the convolution of two peaks. This anomaly corresponds to the onset of magnetic ordering and a crystallographic transition. Further, Figs. 3 and 4 reveal that our results vary systematically with temperature from 1 K to 250 K and follow the similar trend as is exhibited by the experimental data [2,33].

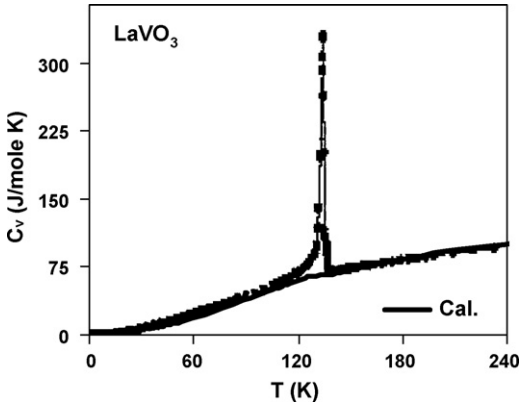

Fig. 3. Variation of specific heat of $LaVO_3$ as a function of temperature. The solid line is the present model calculation for lattice contribution and the line with solid symbols shows the experimental data [2].

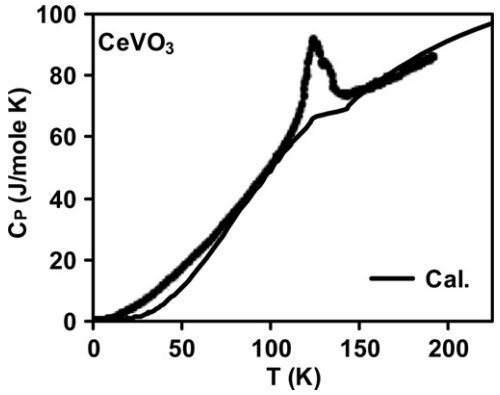

Fig. 4. Variation of heat capacity of $CeVO_3$ as a function of temperature. The solid line is the present model calculation and the line with solid symbols shows the experimental data of Munoz et al. [33].

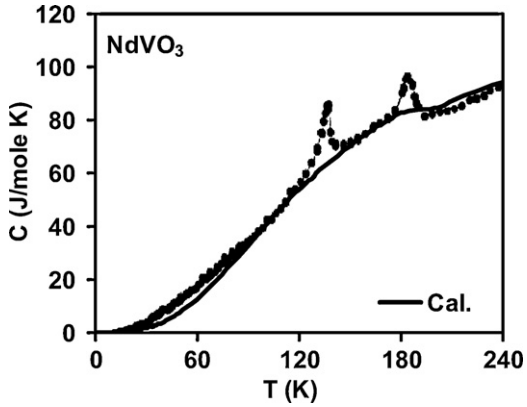

Fig. 6. Variation of specific heat for $NdVO_3$ with temperature. The solid line is the present model calculation and the line with solid symbols shows the experimental data of Tung et al. [2].

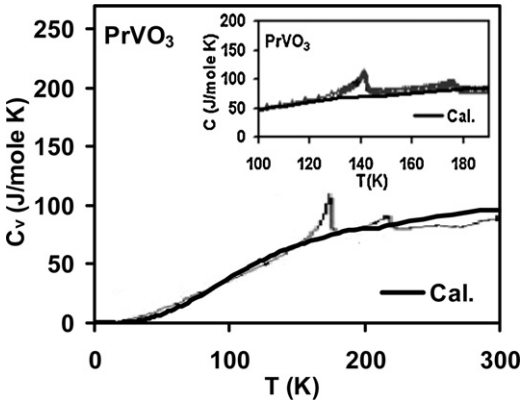

Fig. 5. Variation of specific heat of $PrVO_3$ as a function of temperature compared with the results of Fujioka et al. [34]. Inset shows the specific heat of $PrVO_3$ in the intermediate temperature range ($100\,K \leq T \leq 200\,K$) compared with the experimental results of Fujioka et al. [9]. The solid line is the present model calculation for lattice contribution and the line with solid symbols shows the experimental data.

The agreement between theoretical and experimental results below room temperature in the case of $PrVO_3$ and $NdVO_3$ are similarly good as are seen from Figs. 5 and 6. However the experimental curves for $PrVO_3$ [9,34] and $NdVO_3$ [2] indicate that there are magnetic transitions below 200 K. Since, our computations take account of only the phonon contribution to the specific heat, therefore, these anomalies, arising due to the spin and orbital ordering are not revealed from our calculated specific heat results. But, the specific heat contribution due to the lattice vibrations plays an equally important role in estimating the magnetic contribution to the specific heat curve under a zero magnetic field. The Debye temperature used for calculating the low temperature specific heat is quite different from the Debye temperature at which the specific heat reaches its saturation value. Similar findings were reported earlier also [16,17]. It is also established that, for compounds whose low temperature (LT) Debye temperature (θ_D) is different from the high temperature (HT) Debye temperature, a Debye model with one Debye temperature (LT) does not account for all of the specific heat, as the contribution of optical phonons at higher temperature cannot be neglected and some other formulation such as the Einstein model is needed to account for the specific heat at higher temperatures. The thermal variation of the specific heat for RVO_3 compounds is computed using three Debye temperatures (low temperature θ_D, θ_D in monoclinic and orthorhombic phases respectively). Hence the three Debye temperature model, for low temperature, above and below the transition temperature, can predict the specific heat of the four RVO_3 compounds satisfactorily over a broader range of temperature. We have found that in the perovskite type RVO_3 series as Debye temperature increases (Fig. 2) with change of R, the specific heat correspondingly decreases with decreasing ionic radii except for the compound $CeVO_3$ where specific heat is slightly more than that of $LaVO_3$.

Also, from the view point of exploring the thermal properties of RVO_3 (R = La, Ce, Pr, Nd) compounds thoroughly we have computed the volume thermal expansion at very low temperature ($T = 5$ K) in monoclinic phase and at room temperature in orthorhombic phase using the well known relation $\alpha = \gamma C_V / B_T V$ where B_T, V, C_V are the isothermal bulk modulus, unit formula volume and specific heat at constant volume respectively and γ is the Gruneisen parameter. As the temperature is increased, the atoms in the crystal vibrate more and this corresponds to the material expanding as more volume is taken up by the vibrations. Similar behavior is observed in the present compounds, it can be noticed from Fig. 7 that the value of volume thermal expansion at room temperature is high

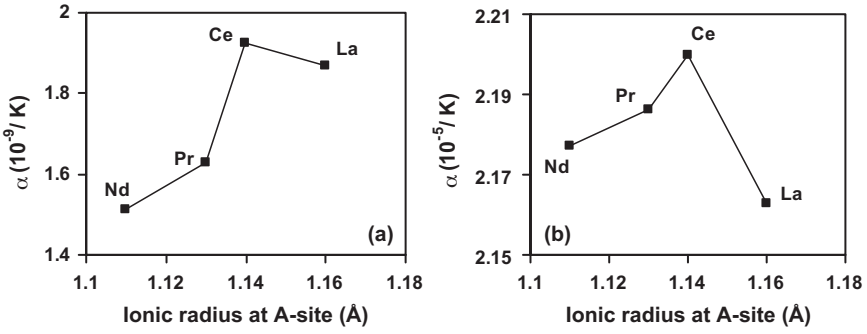

Fig. 7. Volume thermal expansion of RVO_3 (a) at low temperature ($T = 5$ K) (b) and at room temperature as a function of the A-site cation radii.

compared to that of low temperature values and also the thermal expansion follows the same trend as specific heat with decreasing ionic radii for the RVO_3 (R = La, Ce, Pr, Nd) compounds. The volume thermal expansion could not be compared due to lack of experimental data but these values are similar to those often found in ABO_3 type perovskites.

4. Conclusions

In summary, the thermal properties have been systematically and comprehensively investigated using the MRIM to reveal (i) cohesive energy in both monoclinic and orthorhombic phase of the present perovskite type Orthovanadates. (ii) The computation of the bulk modulus of structurally complex materials from atomistic approach involving semiemperical interatomic potential. Our calculated Debye temperature, Gruineisen parameter and specific heat at various temperatures using MRIM have reproduced well almost all the available data. The thermodynamical calculations of structurally complex vanadates emphasize the role of theoretical models for the investigation of panorama of macroscopic physical properties. On the basis of an overall discussion it may be concluded that the MRIM is adequately capable of giving satisfactorily prediction of the bulk modulus, thermal and cohesive properties of the RVO_3 (R = La, Ce, Pr, Nd) perovskites in both monoclinic and orthorhombic phases at various temperatures. The results on specific heat can further be improved by taking into account the *G*-type orbital ordering and *C*-type spin ordering contribution in the interaction potential. Some of the thermodynamic properties reported here are at present of academic interest and they will serve as guide to experimental workers in future.

Acknowledgments

The authors are thankful to University Grants Commission (UGC), New Delhi for providing financial support. One of us Atahar Parveen is thankful to Department of Science and technology (DST) for awarding WOS – 'A'.

References

[1] M.J. Martínez-Lope, J.A. Alonso, M. Retuerto, M.T. Fernández-Díaz, Inorg. Chem. 47 (2008) 2634.
[2] L.D. Tung, M.R. Lees, G. Balakrishnan, D.M. Paul, Phys. Rev. B 75 (2007) 104404.
[3] L.D. Tung, A. Ivanov, J. Schefer, M.R. Lees, G. Balakrishnan, D.M. Paul, Phys. Rev. B 78 (2008) 054416.
[4] L.D. Tung, Phys. Rev. B 73 (2006) 024428.
[5] L.D. Tung, M.R. Lees, G. Balakrishnan, D.M.K. Paul, Phys. Rev. B 76 (2007) 064424.
[6] M.H. Sage, G.R. Blake, C. Marquina, T.T.M. Palstra, Phys. Rev. B 76 (2007) 195102.
[7] Y. Ren, A.A. Nugroho, A.A. Menovsky, J. Strempfer, U. Rutt, C.W. Kimball, F. Iga, T. Takabatake, Phys. Rev. B 67 (2003) 014107.
[8] M. Reehuis, C. Ulrich, P. Pattison, M. Miyasaka, Y. Tokura, B. Keimer, Eur. Phys. J. B 64 (2008) 27.
[9] J. Fujioka, T. Yasue, S. Miyasaka, Y. Yamasaki, T. Arima, H. Sagayama, T. Inami, K. Ishii, Y. Tokura, Phys. Rev. B 82 (2010) 144425.
[10] S. Ishihara, Phys. Rev. B 69 (2004) 075118.
[11] G.R. Blake, A.A. Nugroho, M.J. Gutmann, T.T.M. Palstra, Phys. Rev. B 79 (2009) 045101.
[12] J.S. Zhou, J.B. Goodenough, J.Q. Yan, J.G. Cheng, K. Matsubayashi, Y. Uwatoko, Y. Ren, Phys. Rev. B 80 (2009) 224422.
[13] J.S. Zhou, J.B. Goodenough, Phys. Rev. Lett. 99 (2007) 156401.
[14] S. Miyasaka, Y. Okimoto, M. Iwama, Y. Tokura, Phys. Rev. B 68 (2003), 100406(R).
[15] F. Wang, J. Zhang, J. Yuan, Q. Yan, P. Zhang, J. Phys. Condens. Matter 12 (2000) 3037.
[16] S. Archana, N.K. Gaur, J. Phys. Condens. Matter 21 (2009) 096001.
[17] S. Archana, N.K. Gaur, J. Magn. Magn. Mater. 321 (2009) 3854.
[18] A. Parveen, S. Archana, N.K. Gaur, Int. Ferroelectr. 121 (2010) 129.
[19] D.W. Hafemister, W.H. Flygare, J. Chem. Phys. 43 (1965) 795.
[20] J.C. Slater, J.G. Kirkwood, Phys. Rev. 37 (1931) 682.
[21] L. Pauling, Nature of the Chemical Bond, Cornell University Press, Ithaca, NY, 1945.
[22] R.D. Shannon, Acta Crystallogr. A 32 (1976) 751.
[23] S. Yoon, J. Magn. 12 (2007) 108.
[24] R.T.A. Khan, M.J. Akhtar, Solid State Commun. 137 (2006) 110.
[25] L. Glasser, Inorg. Chem. 34 (1995) 4935.
[26] A. Martin Pendas, A. Costales, M.A. Blanco, J.M. Recio, V. Luana, Phys. Rev. B 62 (2000) 13970.
[27] C. Kittel, Introduction to Solid State Physics, 5th ed., Wiley, New York, 1976.
[28] V.M. Goldschmidt, Naturwissenschaften 14 (1926) 477–485.
[29] C.-M. Fang, R. Ahuja, Phys. Earth Planet. Interiors 157 (2006) 1.
[30] K. Leinenweber, Y. Wang, T. Yagi, H. Yusa, Am. Miner. 79 (1994) 197.
[31] M. Reehuis, C. Ulrich, P. Pattison, B. Ouladdiaf, M.C. Rheinstädter, M. Ohl, L.P. Regnault, M. Miyasaka, Y. Tokura, B. Keimer, Phys. Rev. B 73 (2006) 094440.
[32] P.G. Radaelli, S.W. Cheong:, Phys. Rev. B 66 (2002) 094408.
[33] A. Munoz, J.A. Alonso, M.T. Casais, M.J. Martınez-Lope, J.L. Martınez, M.T. Fernandez-Diaz, Phys. Rev. B 68 (2003) 144429.
[34] J. Fujioka, S. Miyasaka, Y. Tokura, Phys. Rev. B 72 (2005) 024460.